RSC Advances

PAPER

View Article Online
View Journal | View Issue

Cite this: *RSC Adv.*, 2015, **5**, 88425

Simultaneous electronic and ionic conduction in ionic liquid imbibed polyacetylene-like conjugated polymer films†

Arvind Sreeram,[a] Sitaraman Krishnan,*[a] Stephan J. DeLuca,[b] Azar Abidnejad,‡[a] Michael C. Turk,[c] Dipankar Roy,[c] Elham Honarvarfard[d] and Paul J. G. Goulet[d]

Received 21st July 2015
Accepted 8th October 2015

DOI: 10.1039/c5ra14360h

www.rsc.org/advances

Polymer films composed of a polyacetylene-like conjugated polymer and 1-propyl-3-methylimidazolium iodide ionic liquid (IL) were synthesized using a 'one-pot' hydroiodic acid catalyzed thermal dehydration of poly(vinyl alcohol) (PVA) precursor polymer blended with the IL. The dehydration of the precursor polymer and the formation of polyene segments, in films reacted at temperatures in the range of 60 to 250 °C, were characterized using thermogravimetry and infrared spectroscopy. In reactions catalyzed by HI, infrared, ^{13}C NMR, and Raman spectroscopies confirmed nearly complete elimination of the hydroxyl groups of PVA at 200 °C, which was below the decomposition temperature of the IL in the blend. In contrast, the synthesis of the polyene–IL blend was not feasible in the absence of the HI catalyst, because pure PVA exhibited peak mass loss at about 280 °C, a temperature at which the IL also showed significant thermal degradation. Electrochemical and mechanical properties of the polyene–IL blends synthesized at 200 °C were investigated. The films exhibited both electronic and ionic conductivities. The charge conduction pathways were identified and quantified using electrochemical impedance spectroscopy (EIS). The electronic and ionic conductivities increased by as much as four orders of magnitude over the temperature range of 25 to 115 °C. The storage and loss moduli of the films were measured using dynamic mechanical analysis (DMA), and elongation at break was determined by tensile testing. Addition of IL to the conjugated polymer not only imparted ionic conductivity to the polyene films, but also greatly improved their mechanical properties, including the elongation at break.

Introduction

Conjugated polymers have been extensively studied for over three decades[1–3] for use in applications ranging from photovoltaic devices,[4] organic light emitting diodes,[5] and organic thin film transistors.[6] Polyacetylene is among the earliest studied conjugated polymers that demonstrated metal like electron conductivity,[7] and has been synthesized *via* various chemical routes including polymerization of the acetylene monomer using transition metal catalysts,[8] ring opening polymerization of cyclooctatetraene,[9] and thermal conversion of precursor polymers.[10–13] Conjugated polymers are now being actively explored as functional materials in electrochemical energy conversion and storage devices,[14–17] some of which require them to exhibit ionic conductivity in addition to the electronic conductivity afforded by electron delocalization in the π-conjugated polymer segments. For example, materials exhibiting such dual-conductivity have been developed for lithium ion batteries.[18–20]

There are few reports in literature on polymer systems that can exhibit both electronic and ionic conductivities.[20–25] Costantini *et al.*[23] studied polypyrroles with poly(ethylene glycol) (PEG) side chains and investigated the electrical conductivity of these polymers, doped with different concentrations of lithium triflate (LiOTf), using electrochemical impedance spectroscopy (EIS). However, only the overall conductivities of the blends were reported (based on the limiting values of the real part of the complex conductivity *vs.* frequency data), while the individual electronic and ionic contributions to these conductivities remained unresolved. Witker and Curtis[22] reported studies on polythiophenes with PEG side chains. These PEGylated polythiophenes were blended with LiOTf for ionic conductivity and with nitrosonium tetrafluoroborate ($NOBF_4$) for electronic conductivity. Room temperature conductivities in the range of 10–40 μS cm^{-1} were obtained, but the doped polymers were found to lack good film-forming properties. Javier *et al.*[20] studied dual-conducting poly(3-

[a]*Department of Chemical and Biomolecular Engineering, Clarkson University, Potsdam, New York, 13699, USA. E-mail: skrishna@clarkson.edu; Fax: +1-315-268-6654; Tel: +1-315-268-6661*

[b]*Energy Materials Corporation, Norcross, Georgia, 30071, USA*

[c]*Department of Physics, Clarkson University, Potsdam, New York, 13699, USA*

[d]*Department of Chemistry and Biomolecular Science, Clarkson University, Potsdam, New York, 13699, USA*

† Electronic supplementary information (ESI) available: Scanning electron microscopy, electrochemical impedance spectroscopy fit parameters. See DOI: 10.1039/c5ra14360h

‡ Currently at Solvay USA Inc., Vernon, Texas, 76384, USA.

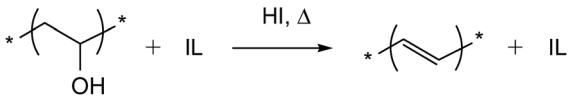

Scheme 1 Synthesis of polyene film containing 1-propyl-3-methylimidazolium iodide IL by heating a solvent-cast precursor film at elevated temperature and at ambient pressure or in vacuum. Idealized polyene structure is shown. Actual structure would contain sp^3 defects resulting from side reactions such as Diels–Alder addition and free radical crosslinking.

hexylthiophene)-*b*-poly(ethylene oxide) (P3HT-*b*-PEO) block copolymers, containing dissolved $LiPO_4$ salt, for use in Li ion batteries. The simultaneous presence of both ionic and electronic conduction rails in these materials was detected using EIS. Lin *et al.*[26] studied the ion transport mechanism in cationically and anionically functionalized polyacetylene ionomers. The ionic conductivity measured by them using EIS was found to exhibit an Arrhenius dependence on temperature. However, these polymers were associated with a fairly low intrinsic electronic conductivity ($\sim 10^{-9}$ mS cm^{-1} near room temperature).

Firestone and coworkers investigated mesostructured π-conjugated polyelectrolytes prepared by polymerization of bifunctional ionic liquid (IL) monomers.[27–29] In one study, an imidazolium bromide IL with dodecyl and propargyl groups was polymerized using a rhodium-based initiator, in aqueous phase, wherein the amphiphilic IL self-assembled to form a hexagonal perforated lamellar structure.[27] A film of the polymer prepared by spraying the polymer on a glass substrate was found to consist of lamellar microstructures and have a conductivity of 70.2 μS cm^{-1} at room temperature. The polymer was stable against oxidation, and the conductivity decreased only slightly upon long-term storage. Ionomers containing thienyl moieties were also reported.[28,29] The alkyl thiophene ionomers exhibited significantly higher conductivity than the acetylene ionomers. Only room temperature values of the overall conductivities were studied; the ionic and electronic contributions were not investigated.

To our knowledge, there are no reports on the electrical and mechanical properties of films prepared from blends of conjugated polymers and ILs. In the work reported herein, films consisting of polyacetylene-type conjugated polymer and 1-propyl-3-methylimidazolium IL blends were synthesized using an acid-catalyzed dehydration of poly(vinyl alcohol) (PVA) precursor (Scheme 1). The chemical structure of the resulting polymer–IL film was characterized using IR, Raman, and ^{13}C NMR spectroscopy. The individual electronic and ionic conduction pathways supported by these films were identified and quantified using EIS. Tensile strength and elongation at break were determined by tensile testing of free-standing films. The storage and loss moduli of the films were measured using dynamic mechanical analysis (DMA).

Experimental

Materials

Poly(vinyl alcohol) (PVA, CAS no. 9002-89-5, Aldrich, average mol. wt 146 000–186 000 g mol^{-1}), hydroiodic acid (HI, CAS no. 10034-85-2, Aldrich, ACS reagent, 47 wt% solution in water, <1.5% hypophosphorous acid stabilizer), 1-methyl imidazole (CAS no. 616-47-7, Aldrich, 99%), 1-iodopropane (CAS no. 107-09-4, Aldrich, 99%), ethanol (EtOH, Pharmco-AAPER, 200 proof, anhydrous), diethyl ether (Aldrich, 99%), and *N*,*N*-dimethylformamide (DMF, J. T. Baker, 99.8%) were used as received. Ultrahigh purity nitrogen (Airgas, 99.999% purity, <1 ppb oxygen and water) and deionized water were used for all experiments.

Methods

Synthesis of polyene–IL composite films. 1-Propyl-3-methylimidazolium iodide IL, was synthesized using a previously reported method,[30] and dried under vacuum at 125 °C. A 5 wt% PVA solution was prepared by dissolving the polymer in an ethanol–water solution (*cf.* recipe in Table 1) and stirring at 80 °C for one hour. An equimolar amount of hydroiodic acid was added dropwise to the polymer solution, followed by the addition of the desired amount of IL in three different concentrations (Table 1). The resulting mixture was dried on a polytetrafluoroethylene (PTFE) substrate at 60 °C under vacuum for 12 h, to form the precursor film. The precursor films were converted at 200 °C in a custom-built air-tight reactor that contained a temperature controlled heating stage and ports connected to nitrogen and vacuum lines.[31] All films were converted at a reduced pressure (~10 mmHg) using a PTFE dry vacuum pump.

Characterization methods. Thermogravimetric (TG) analysis of the polymer films was performed using a Pyris 1 Thermogravimetric Analyzer (PerkinElmer, Waltham, MA). The sample (approx. 10 mg) was heated in a Pt pan under nitrogen purge (20 cm^3 min^{-1} standard ambient temperature and pressure), at a constant heating rate of 10 °C min^{-1} from 50 °C to 600 °C. Differential scanning calorimetry (DSC) data for films F0, F1, and F2, reacted at 200 °C for 1 h, were acquired using a Q100 DSC (TA instruments, Milford, MA). The sample for DSC was heated and cooled in closed aluminium pan, having a pinhole in the lid, at a constant rate of 10 °C min^{-1}, over the temperature range of −80 °C to 200 °C. Data were collected over two heating and cooling cycles.

The IR spectra of the polymer–IL blends were obtained using a Spectrum 100 FTIR spectrometer (PerkinElmer, Waltham, MA) in the transmission mode. Films of the precursor polymer were cast on a polystyrene Petri dish and dried at 60 °C in vacuum for 12 h. The films were then peeled off and heated at the temperature of interest in the preheated evacuated reactor.

Table 1 Composition of solutions, in relative amounts by mass, used for casting precursor films F0, F1, and F2

	F0	F1	F2
PVA	1.00	1.00	1.00
Ethanol	3.15	3.15	3.15
Water	15.85	15.85	15.85
HI sol.[a]	6.18	6.18	6.18
IL	0	0.25	0.50

[a] The hydroiodic acid solution contained 47 wt% of HI.

The films were heated directly on Al sample holders that could then be inserted in the IR spectrometer for data acquisition.

^{13}C cross polarization magic angle spinning (CPMAS) solid-state NMR spectra were acquired using a Varion Inova 400 spectrometer operating at a ^{13}C frequency of 100 MHz. Approximately 100 mg of the solid films were used for each measurement.

Raman scattering spectra were collected in a backscattering geometry with 514.5 nm laser excitation using a Renishaw inVia Raman microscope. The laser was focused onto the samples using a 20× microscope objective, and laser powers at the sample were between 50 and 100 μW. Higher laser powers were found to damage samples. The samples for these studies were prepared on 1 × 1 in glass slides and dried at 60 °C for 12 h in vacuum. The precursor films were reacted at 200 °C in the evacuated reactor to obtain the conjugated polymer films for analysis. All reported spectra were obtained with a minimum of 10 accumulation runs.

The IR, NMR, and Raman spectroscopy analyses were conducted at ambient temperature and pressure.

Film surfaces were analyzed using field emission scanning electron microscopy (SEM) using a JEOL 7400 High Resolution Field Emission Electron Microscope. Prior to analysis, samples were sputter-coated with approximately 60 Å thick Au/Pd layer.

Mechanical testing of the polymer films was carried out using a dynamic mechanical analyzer (Q800, TA instruments, Milford, MA). The samples tested were of approximately 10 mm in length, 5 mm in width and 0.2 mm in thickness. The frequency sweep experiments were performed over a range of 1 to 80 Hz using 0.1% strain amplitude and 1 mN preload force and a tension film clamp. The stress *vs.* strain data were acquired by increasing the stress at a constant rate of 0.1 N min^{-1} until the sample broke. All tests were performed at 35 °C in air at ambient pressure.

The conductivities of the polymer films were characterized using EIS over a temperature range of 25 to 115 °C. The free standing film of about 200 μm thickness was sandwiched between two polished stainless steel electrodes, and loaded into an electrochemical cell of steel casing (Two-Electrode Split Test Cell from MTI Corporation). The cell was placed in a temperature-controlled TESTEQUITY 105A environmental chamber. The sample conductivities were measured in 15 °C intervals, and the entire cell was equilibrated at each test temperature for one hour prior to data collection. The test cell was electrically controlled using a Solartron 1287A potentiostat/galvanostat coupled with a model 1252A frequency response analyser. EIS data were recorded as Nyquist plots with AC perturbation voltages of 15 mV amplitude in a frequency range varied between 0.1 Hz and 300 kHz. The experimental Nyquist spectra were validated following a previously reported procedure,[32] and subsequently analysed using complex nonlinear least squares (CNLS) fitting, to determine the appropriate electrical equivalent circuit (EEC) model for conductivity determination. ZSimpWin™ was used for the CNLS fitting calculations. The uncertainties in all the calculated resistance elements were generally confined below about 15%.

All samples were stored in sealed glass containers in the dark. Measurements on the films were performed usually within 2 days after the films were prepared.

Results and discussion

Film preparation

Kozlov and McCarthy investigated two different reactions for the conversion of ultrathin PVA films (coated on PTFE sheets) to polyacetylene: (1) dehydration by $NaHSO_4$ catalyzed pyrolysis; and (2) dehydration by Chugaev reaction, of an *S*-methyl polyvinyl xanthate intermediate.[12] The conversion of the PVA film to xanthate involved reaction with a two-phase system containing NaOH, carbon disulphide, methyl iodide, and a phase-transfer catalyst. The conversion of the xanthate to polyacetylene was found to be possible even at a temperature of 120 °C. The $NaHSO_4$ catalyzed reaction, on the other hand, required a higher temperature of 200 °C. XPS analysis, however, indicated that both approaches were limited to surface groups, and that the film prepared using the xanthate approach retained sulphur that was left after the decomposition of the xanthate.

Maruyama *et al.*[11] studied the kinetics of sulphuric acid and phosphoric acid catalysed dehydration of PVA using UV spectroscopy and found that polyenes with degrees of conjugation up to 13 were formed. They also found that reactions carried out at temperatures of 160, 170, 180, and 190 °C exhibited first order kinetics. The activation energy was lower for the reactions catalysed by H_3PO_4 (∼60 kJ mol^{-1}) compared with those catalysed by H_2SO_4 (∼97 kJ mol^{-1}). However, conductivities of the resulting films were not reported.

In the present study, we used hydroiodic acid as a catalyst for thermal dehydration of PVA. The synthesis is expected to result in the formation of *trans*-polyene segments, the form that is thermodynamically more stable than *cis*-polyene.[33] Unlike the conventional approaches, the precursor films of the present study additionally contained a relatively non-volatile IL to impart ionic conductivity and to improve mechanical properties of the dehydrated films.

Thermal conversion of the precursor film was found to cause partial exclusion of the IL from the polymer matrix. The IL phase-separated in the form of droplets on the film surface. Blotting of these droplets with an absorbent tissue paper (Kimwipe) and mass determination before and after blotting indicated that about 70 ± 5 wt% of the IL present in the precursor film was retained in the reacted sample. The surfaces of the blotted films appeared uniform and did not show evidence of further phase segregation upon storage (*cf.* SEM images in Fig. S1 of ESI†).

The phase separation of IL can be a result of the partial immiscibility of the polar IL with the relatively nonpolar polyene matrix.[34] The IL, however, was fully miscible with the polar PVA in the precursor film. The phase separation of IL is also attributed to the reduction in volume of the polymer matrix that occurs during thermal elimination. Complete conversion of pure PVA to polyacetylene would result in a volume reduction of at least about 41%. The poor mechanical properties of polyacetylene films obtained by the thermal conversion route are often attributed to such large shrinkages after conversion. The presence of IL in our films significantly alleviates the problem of film deformation due to mechanical stress generation during

thermal elimination reaction. Films F1 and F2 were found to have good mechanical properties as will be discussed in the section on mechanical characterization.

Fig. 1 shows TG and derivative TG (DTG) plots for pure PVA, pure IL, and the three precursor films, F0, F1, and F2, containing HI. In the absence of HI, PVA showed a peak in the rate of mass loss at about 280 °C, attributed to the dehydration reaction, and the breakdown of the polymer chain into volatile fragments, which continues at higher temperatures (beyond 400 °C). The IL exhibited a peak in the DTG plot at a temperature of about 317 °C, which is attributed to dealkylation reaction and subsequent volatilization.[30]

In the case of films F0, F1, and F2 that contained HI, the dehydration reaction occurred at a lower temperature, evident from the appearance of a peak (or a shoulder, for sample F2) at a temperature below 200 °C. The fact that HI lowered the temperature required for water elimination is significant, because this allows 'one-pot' synthesis of the IL-imbibed polyene films without causing chemical degradation of the IL in the film. In order to confirm that the IL was not affected by HI, a mixture of the IL and HI solution was heated at 200 °C for 1 h and the HI and water were distilled off from the sample under vacuum. ^{1}H NMR spectrum of the HI-treated IL showed that it was identical to the pristine IL.

The stoichiometric mass loss expected for the dehydration reaction shown in Scheme 1 is 41%. However, film F0, with no IL, showed a higher mass loss, of about 60% at 300 °C (Fig. 1a). The higher than stoichiometric mass loss is attributed to evaporation of HI present in the precursor film, in addition to elimination of water *via* the dehydration reaction. Although a significant amount of HI evaporated from the film during drying, the amount that remained was evidently sufficient to catalyze the dehydration reaction to completion.

With the addition of the IL to the precursor film, the asymptotic value of mass loss (below 400 °C) increased with an increase in the concentration of the IL in the precursor film, which is attributed to greater evaporation of HI from the films containing higher IL concentration. Dilution of the precursor film would increase the rate of removal of HI from the film by increasing the diffusion coefficient of HI in the precursor film. It could also lower the saturation solubility of HI in the film by weakening PVA–HI intermolecular interactions.

The reaction onset temperature, considered as the temperature corresponding to 5% mass loss in the TG data of Fig. 1a, was 141 °C for F0, 157 °C for F1, and 177 °C for F2. The observed increase in the reaction onset temperature with an increase in the IL concentration is consistent with our expectation of lower residual concentration of HI in the heated films containing more IL. Furthermore, the IL can stabilize PVA against dehydration by hydrogen-bonding interactions with the hydroxyl groups of PVA.

As seen from Fig. 1a, pure PVA and pure IL degraded almost completely when the temperature was increased to 600 °C. However, in the presence of HI, films F0, F1, and F2 showed a residual mass of about 16% at 600 °C, attributed to the formation of a thermally stable carbon.

All films reacted at 200 °C were characterized using differential scanning calorimetry, but no characteristic melting or crystallization peak, or glass transition, was observed in the temperature range of −80 to 200 °C in our measurements.

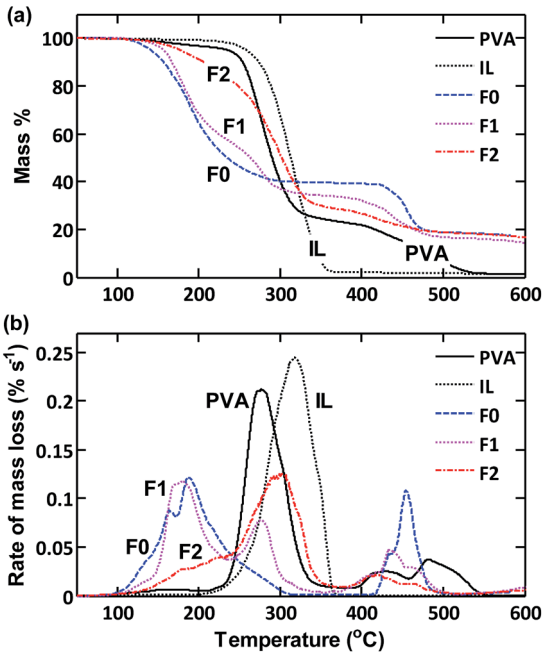

Fig. 1 (a) TG and (b) DTG plots of PVA, IL and precursor films F0, F1 and F2; 10 °C min^{-1} heating rate and 20 cm^3 min^{-1} N_2 purge.

Chemical characterization

Fig. 2 shows FTIR spectra of the precursor films, F0, cast and dried at 60 °C, and further heated at four elevated temperatures in vacuum for 1 h. The film dried at 60 °C showed a strong PVA O–H stretch band at 3300 cm^{-1}. As the reaction temperature was increased, the films underwent elimination of water molecules from the polymer backbone, as seen from the decrease in the intensity of the O–H stretch band. The significant decrease in the intensity of this band due to the dehydration reaction is consistent with the large decrease in sample mass observed in the TGA results (Fig. 1) over this temperature range. The IR spectrum of the film reacted at 250 °C showed almost complete disappearance of the O–H peak. In contrast, when the PVA film was heated at different temperatures in the absence of HI, the intensity of the O–H peak remained high even for the film heated up to 250 °C (spectra not shown), indicating very low conversion in the films at these temperatures.

Arbuckle *et al.*[35] reported that the C–H stretch vibrations in Naarmann polyacetylene occurred at 2959, 2929, and 2871 cm^{-1}, and in the 2960–2850 cm^{-1} range in Tsukamoto polyacetylene. Chen *et al.*[36] studied polyacetylene films with high *trans*-polyene content and observed a strong peak at 3013 cm^{-1}, attributed to the C–H stretch vibrations. The IR spectra of the reacted polymer films (Fig. 2) exhibited peaks at 2923 and 2855 cm^{-1}, in agreement with these previous reports.[35,36] A lower

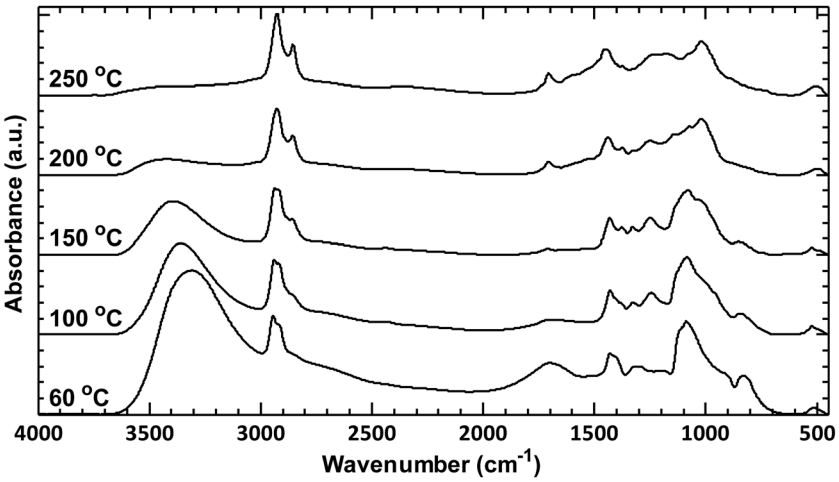

Fig. 2 FTIR spectra of PVA precursor film, F0, heated in vacuum for 1 h at different temperatures.

intensity shoulder observed at 1134 cm^{-1}, is attributed to the C–C stretching of polyacetylene.[37]

The IR spectra of the of the polyene films of the present study showed features similar to those in the spectrum of β-carotene, a small molecule analogue of π-conjugated polymers. β-Carotene is an isoprene-derived hydrocarbon with 11 conjugated mono- and di-substituted C=C bonds. Saito *et al.*[37] conducted IR spectroscopy of β-carotene and reported peaks at 1442 cm^{-1}, assigned to rocking vibrations of the methyl substituents, 1369 cm^{-1}, assigned to C–CH_3 stretching vibrations, 1256 cm^{-1}, assigned to in-plane C–H bending, and 1009 cm^{-1}, assigned to C–C stretching. Similarly, peaks at 1431, 1370, 1247, and 1012 cm^{-1} were observed in the IR spectra of the present study. Mizuno *et al.*[38] studied the IR spectra of iodine-doped β-carotene and found that the sharp peaks in the IR spectra of undoped β-carotene were replaced by broad bands at 1464, 1122 and 972 cm^{-1}. They also found that iodine-doped Shirakawa polyacetylene showed similar broad bands at 1297, 1288 and 888 cm^{-1}. On the basis of these studies, we infer that the films of the present study contain substituted polyenes, wherein the alkyl substituents are derived from Diels–Alder or free-radical addition reactions.[39,40]

Films reacted at 200 and 250 °C showed a small but prominent peak at 1714 cm^{-1}, which could correspond to the C=O stretch vibrations of carbonyl defects in the film,[31] formed by oxidation of the vinyl alcohol groups.[11] However, ^{13}C NMR spectra of these films did not show the presence of C=O carbon atoms. Thus, C=O defects, if present, were of fairly low concentration.

FTIR analysis of the film, F2, which contained the 1-propyl-3-methylimidazolium iodide IL, also showed a significant decrease in the O–H band intensity and development of C–H stretch peaks at 2937, 2919, and 2861 cm^{-1} upon reaction at higher temperatures (spectra not shown). Peaks at 3149 and 3085 cm^{-1}, corresponding to the imidazolium C–H stretch vibrations, and peaks at 1571 and 1166 cm^{-1}, corresponding to the C=N and C–N stretch vibrations, respectively, were additionally observed.

Fig. 3 shows the ^{13}C NMR spectra of film F2 that was dried in vacuum at 60 °C and then reacted at 200 °C for 1 h. The resonance of the CH–OH C atom, seen at 67.8 ppm in spectrum of the precursor film, essentially disappeared after the film was reacted at 200 °C. Furthermore, the peak at 45 ppm in the spectrum of the precursor film, attributed to the CH_2 resonance in PVA,[41] was significantly lower in intensity in the spectrum of the film reacted at 200 °C.

The broad peaks in the 115–150 ppm region of the ^{13}C NMR spectrum of the converted films, are attributed to sp^2 carbons of the polyene segments. Hanková *et al.*[42] observed similar peaks in the polyacetylene-type crosslinked system they studied. These peaks were present in the NMR spectrum of the precursor film as well, indicating that some polyene formation occurred even during drying at 60 °C.

The peak observed at 30 ppm, in the NMR spectrum of film reacted at 200 °C, is attributed to sp^3 C atoms, resulting from side reactions mentioned previously.[39,40] These C atoms, of the tri-substituted type, could result in crosslinking and graphitization of the film,[40] and therefore have a strong effect on the electrical and mechanical properties of the film.

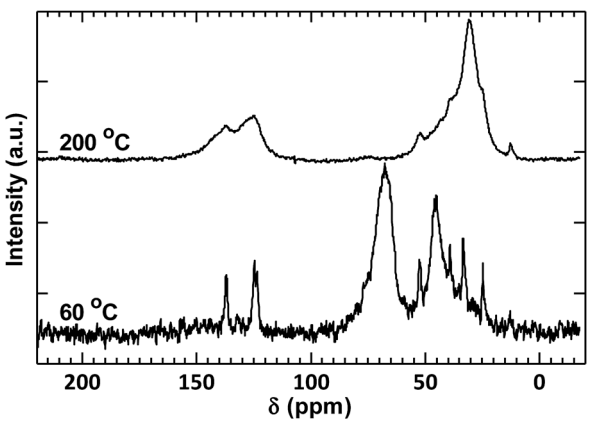

Fig. 3 ^{13}C NMR spectra of film F2, before and after heating in vacuum at 200 °C for 1 h.

Evidence for the presence of conjugated double bonds is further strengthened by Raman spectroscopy experiments. Fig. 4 shows the Raman spectra of the precursor film F2, dried at 60 °C, and of the film after reaction at 200 °C. The precursor film showed only the iodide/polyiodide peaks in the low frequency region of the spectra (below 500 cm^{-1}).[38] The polyiodides are presumably formed from the HI and IL derived iodide. The Raman resonances of the imidazolium iodide IL were absent, or very weak compared with those of the polyene,[43,44] for the laser source and intensity used in this work.

The appearance of two strong bands at 1515 and 1127 cm^{-1} and a weak band at 1003 cm^{-1}, which were absent in the spectrum of the precursor film, confirmed the formation of the conjugated double bonds.[45,46] The bands at 1515 and 1127 cm^{-1} are attributed to the C=C stretching vibrations, and a mixed mode of C–H bending and C–C stretching vibrations, respectively.[46]

Shirakawa *et al.*[45] reported the Raman spectra of *trans*- and *cis*-polyacetylene, with the *trans*-polyene having similar strong bands at 1474 and 1080 cm^{-1} and a weak band at 1016 cm^{-1}, when a 632.8 nm Raman source was used. They were unable to obtain the spectrum of pure *cis*-polyacetylene because *cis–trans* isomerization occurred during the measurement, due to heating by the laser irradiation, resulting in *trans* bands at 1500, 1100, and 1016 cm^{-1} along with the *cis* bands at 1552, 1262 and 920 cm^{-1}. The *cis* bands disappeared when an intense 488 nm laser source was used, due to complete isomerization.

Harada *et al.*[46] acquired Raman spectra of Shirakawa polyacetylene films using a 488 nm laser excitation, and reported bands at 1492, 1116, and 1007 cm^{-1}. They estimated the presence of long *trans*-polyene segments with degree of conjugation greater than 100. The shifts to higher wavenumbers, of the Raman bands in our spectrum, is attributed to a lower conjugation length of C=C bonds in our films as compared with the Shirakawa polyacetylene.

The position of the C=C resonance in the Raman spectrum of a polyene is dependent on the conjugation length and stereoisomerism of the polyene, and on the excitation wavelength used. For the *trans* isomer, the C=C Raman shift increases significantly with a decrease in the degree of conjugation,[47] and increases slightly with a decrease in the wavelength of the Raman source.[46] Using *trans*-polyene homologs of known chain lengths, Harada *et al.*[47] have reported a correlation between the Raman shift of the C=C peak, and the conjugation length. Using their empirical correlation, we estimated the conjugation length of the polyene formed in our films to be close to 10, similar to that in β-carotene. The presence of IL during the dehydration reaction did not have a significant effect on the degree of conjugation of the polyene formed.

Mechanical characterization

Polyacetylene is a brittle polymer,[48] and its poor mechanical properties greatly limits its utility. Some approaches to overcome this problem have been previously reported. Galvin *et al.*[49] used *in situ* polymerization of acetylene in low density polyethylene films impregnated with a Ziegler–Natta catalyst to obtain a blend with improved tensile strength and elongation at break. Using a similar approach, Rubner *et al.*[50] prepared blends of polyacetylene and 1,4-polybutadiene. They found that the elastic range, determined using a cyclic loading and unloading procedure, decreased as the polyacetylene content of the blends increased. At high polyacetylene levels (greater than 40 wt%), the samples underwent almost complete plastic deformation, which they attributed to an increased rigidity resulting from the crystalline polyacetylene microdomains. To our knowledge, the use of an IL as a binder and plasticizer for conjugated polymers has not been previously reported. We found that the incorporation of an IL such as 1-propyl-3-methylimidazolium iodide is an effective approach to improve the mechanical properties of conjugated polymer films, while also imparting ionic conductivity to these films. Fig. 5 shows a photograph of a free-standing flexible film (of composition F2), resulting from the addition of the IL to the polymer.

Fig. 6 and 7 show the results of dynamic mechanical analysis (DMA) of films F0, F1, and F2 dried at 60 °C and subsequently heated at 200 °C. The DMA experiments were performed at 35 °C (Fig. 6) and at 115 °C (Fig. 7). The storage modulus and loss modulus, E' and E'', respectively, of the films were measured as a function of the frequency, over a range of 1 to 80 Hz, and a strain amplitude of 0.1%. At 35 °C, these values were found to be relatively independent of frequency. The average values are reported in Fig. 6 along with the standard deviation (as error bars). The E' and E'' values of the precursor polymer film were

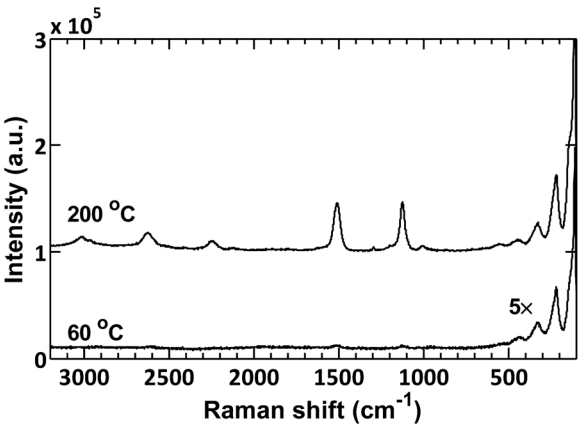

Fig. 4 Raman spectra of film F2, before and after heating in vacuum at 200 °C for 1 h; spectra acquired using 514.5 nm excitation wavelength.

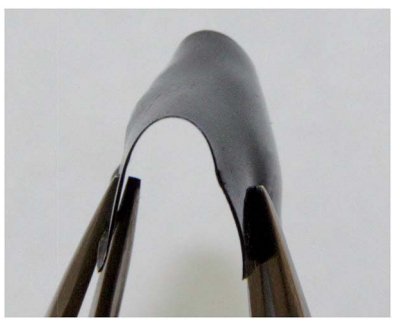

Fig. 5 Photograph of film F2 after reaction at 200 °C. The image shows the film flexed between pairs of tweezers at room temperature.

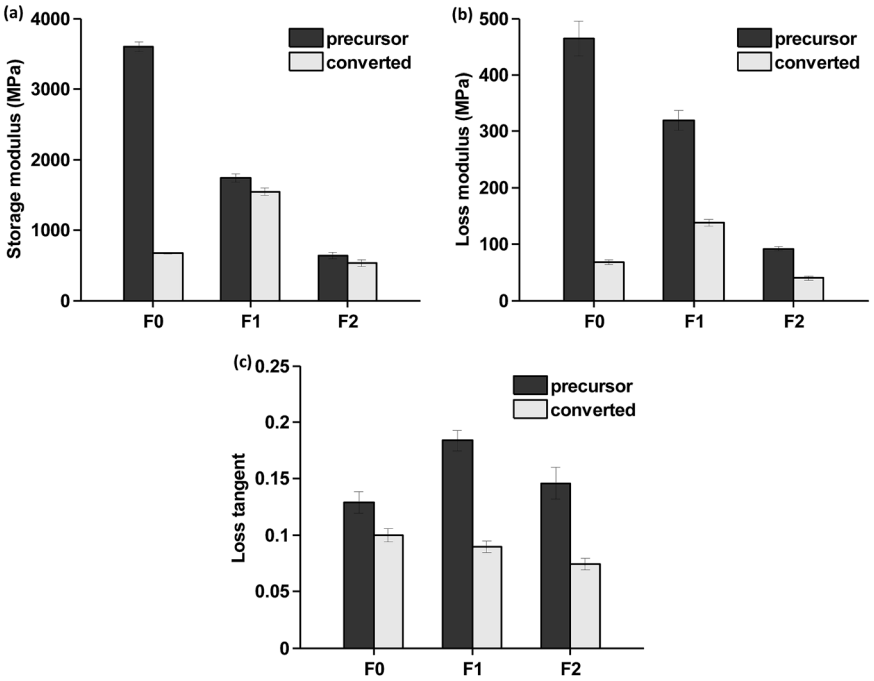

Fig. 6 DMA results of the precursor and converted films, F0, F1, and F2, at 35 °C: (a) storage modulus, (b) loss modulus, and (c) loss tangent; 1% oscillation amplitude, and 1 to 80 Hz frequency.

around 3 GPa and 500 MPa respectively, while after reaction at 200 °C, these decreased to 700 and 65 MPa, respectively. The significant drop in modulus is attributed to the partial or complete loss of crystallinity (pure PVA is semicrystalline) and also to the formation of voids and cracks in the film because of volume shrinkage during conversion.

The precursor films F1 and F2 that contained the IL showed lower E' and E'' compared with F0, because of the presence of liquid inclusions, as expected. However, after reaction at 200 °C, both E' and E'' of the films containing the IL, F1 and F2, were similar to, or higher than the pure polyene film F0 (*cf.* modulus values of F0 and F1, and F0 and F2, in Fig. 6). Although the presence of a liquid component in the film would lead to a decrease in modulus, the modulus increased (or decreased only slightly in the case of F2), evidently because the IL relieved mechanical stresses during conversion and prevented the formation of voids and cracks.

The E', E'' and loss tangent ($\tan\delta = E''/E'$) values of the reacted films at 35 °C showed a non-monotonic trend with IL concentration due to these opposing effects: a decrease in modulus because of an increase in the amount of liquid component and an increase in modulus because of fewer morphological defects (voids or cracks) in the film.

Fig. 7 shows the frequency dependence of the values of E', E'', and $\tan\delta$ of the films measured at 115 °C. Film F0, without the IL, showed negligible frequency dependence even at this higher temperature. However, films F1 and F2 showed an increase in the values of E' and E'' with frequency, characteristic of materials at temperatures in the vicinity of the glass–rubber transition temperature. Note, however, that the glass transition, if present in the temperature range of −80 to 200 °C, was too weak to be detected in our DSC experiments.

For films containing the IL, $\tan\delta$ values were higher at 115 °C than at 35 °C (*cf.* Fig. 7c and 6c), because of an increase in

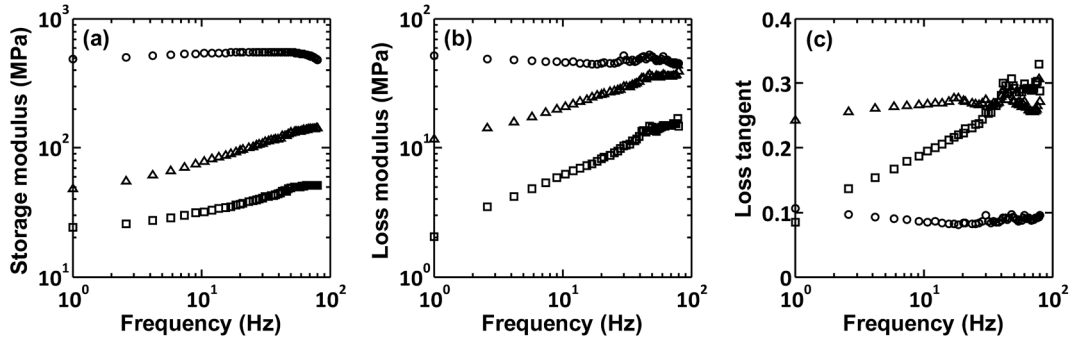

Fig. 7 DMA results of fully-dehydrated films, F0 (○), F1 (△), and F2 (□), at 115 °C: (a) storage modulus, (b) loss modulus, and (c) loss tangent; 1% oscillation amplitude.

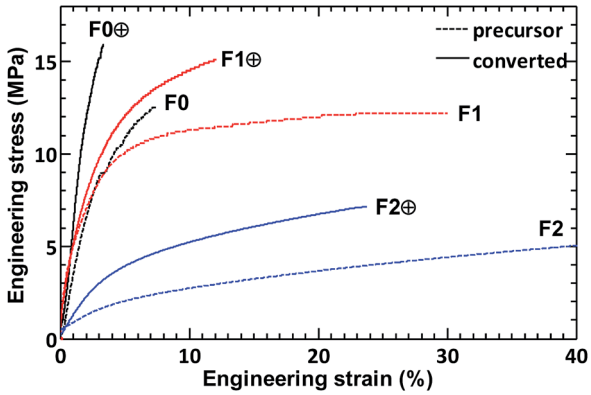

Fig. 8 Stress *vs.* strain data for the precursor and converted films (⊕) acquired at 35 °C in the tensile mode. Precursor film F2 showed strain of about 106% before failure, but the scale of the strain axis is truncated for clarity.

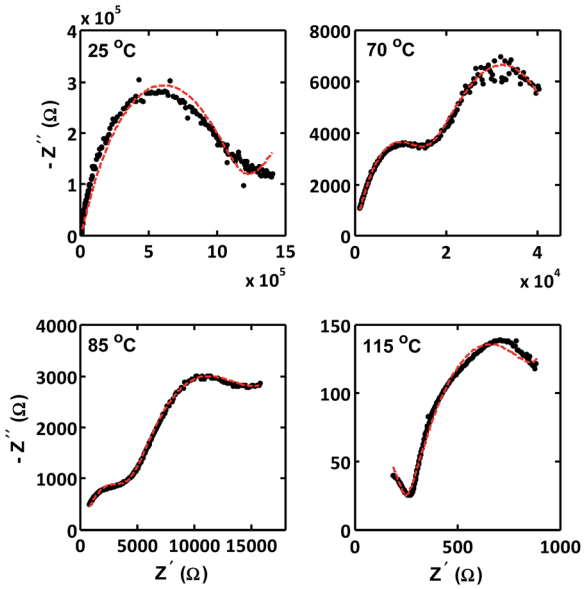

Fig. 9 EIS Nyquist plots for fully converted film F2, at representative temperatures of 25, 70, 85, and 115 °C. Dots are experimental data and the smooth lines are best-fit curves to the EEC model shown in Fig. 10.

viscous dissipation with an increase in temperature. However, film F1, with a lower concentration of IL showed a higher tan δ, which was relatively independent of frequency, than film F2, which showed an increase in tan δ with an increase in frequency. These effects are obviously related to intermolecular interactions between the polyene network and the IL, and need further investigation.

Fig. 8 shows the tensile stress–strain plots for the polymer–IL films, measured at 35 °C. In these experiments the stress was increased at a constant rate of 0.1 N min^{-1} and the elongation was recorded until break (EOB, Table 2). Data for the precursor films (dried at 60 °C) and thermally converted films (heated at 200 °C for 60 min) are shown. The addition of 20 and 33 wt% of IL to the precursor film (samples F1 and F2, respectively) led to 350 and 1500% increase in EOB in the case of the precursor film, and 250 and 600% increase in EOB, respectively, for the reacted films. The toughness of the films also increased upon addition of the IL to the films. The values of the modulus of toughness (the area under the stress–strain curve) are compared in Table 1. After conversion, film F1 was about 4.4 tougher than film F0, which did not contain the IL. Film F2 exhibited a slightly lower toughness than film F1. Obviously, there is an upper limit on the IL concentration in the film for obtaining the desired increase in toughness.

Electrical characterization

Fig. 9 shows the Nyquist plots for film F2 at four representative temperatures. In these plots Z' (abscissa) and Z'' (ordinate) are the real and imaginary components of the complex impedance, Z, measured at different frequencies, ω. Good fits to EIS data were obtained, for all temperatures (correlation coefficient, r^2, between the measured and calculated impedance components was greater than 0.99, except in the case of the Z'' values at 25 °C, for which r^2 was about 0.967).

Polyacetylene is prone to air oxidation especially in the presence of water,[51] but its oxidation has been found to be prevented by the introduction of stable doping ions such as I^-, F^-, or BF_4^-.[52] The observation by Ringstrand *et al.*[27] that their polyacetylene ionomer films, which contained Br^- ions, resisted oxidation upon storage in air is consistent with the prior reports[52] on ion-imparted stability. In the present study, EIS measurements were repeated at different times to check temporal variation of the data. The Nyquist spectra recorded at a given temperature, but at different times, resulted in nearly the same EEC fit parameters, which confirmed the absence of significant (bulk and/or interfacial) changes in the sample properties due to air or water interactions. Furthermore, the samples were equilibrated at 115 °C before EIS measurements, so that any degradative reaction that could be promoted by

Table 2 Elongation at break (EOB, %) and modulus of toughness (MJ m^{-3}) of precursor and reacted films measured at 35 °C, using tensile stress–strain analysis

		Elongation at break		Modulus of toughness	
Sample	IL content of precursor film (wt%)	Precursor film, dried at 60 °C	Film reacted at 200 °C	Precursor film, dried at 60 °C	Film reacted at 200 °C
F0	0	6.8	3.4	0.63	0.31
F1	20	30.0	12.1	3.12	1.39
F2	33.3	106.3	23.7	5.72	1.22

temperature would not affect subsequent measurements at lower temperatures.

In EIS measurements, a pure electronic or pure ionic conduction rail would typically display a single-arc Nyquist plot. In the present work, a trailing low-frequency (high impedance) feature of the main Nyquist arc could be seen in data acquired at the lower temperatures (*cf.* the Nyquist plot for the 25 °C in Fig. 9), which eventually develops into a second arc (seen clearly in the 70 °C data in Fig. 9). This feature is indicative of two different time constants, one associated with electronic conduction and the other with ionic conduction.

The EEC used for the analysis of the data (Fig. 10) was a slight modification of the circuit models proposed by Płocharski *et al.*[24] and Javier *et al.*[20] for mixed-conduction polymeric systems. This EEC, which is a generalized Maxwell's circuit model,[53] consisted of a constant phase element (CPE), Q_c, in series with the main circuit, to account for the interfacial impedance between the stainless steel electrodes and the polymer film. In general, the contact impedance established between two such materials, of very different electronic conductivities, can be modelled by the parallel combination of a contact resistance and a contact CPE (or capacitance).[54] The absence of such a contact resistance in the EEC of Fig. 10 indicated that this resistance was considerably large for the films of the present study,[55] and was, therefore, shunted out by Q_c. Note that the contact CPE in the EEC is D. C. blocking for both electrons and ions, and responds to electron transport only under A. C. perturbation.

The main circuit denoting the polymer sample contained the resistances R_e and R_i, corresponding to the ohmic paths of electrons and ions, respectively. In this part of the EEC, Q_0 represented the geometric CPE (frequency dispersed capacitance) of the polymer film, and Q_i represented the ionic double layer, characteristic of the polymer/IL at the film–electrode interface.

The Nyquist spectra generally consisted of two visually separable impedance arcs, arising from the electronic and the ionic rails considered in the EEC (for example, see the spectra acquired at 70 and 85 °C in Fig. 9). The arc corresponding to electronic conduction was identified on the basis of the characteristic frequency of the Q_0–R_e combination, calculated using the CNLS-fitted parameters (Table S1 in ESI†). The procedure used for this analysis is described in the ESI.† As discussed there, the impedance arc appearing on the left side (high-frequency data) of the Nyquist spectrum corresponds to the electronic rail, while the structure on the right side (low-frequency data) represents the ionic rail. The detailed structure of the electronic arc was found to be particularly sensitive to temperature changes. This high-frequency structure systematically shrunk in size, and shifted to the left, toward the $-Z''$ axis, as the EIS measurement temperature was increased. As a result, the impedance spectra recorded at 115 °C predominantly displayed the impedance features of the ionic rail. Conversely, the spectra recorded at 25 °C showed mainly the characteristics of the electronic rail.

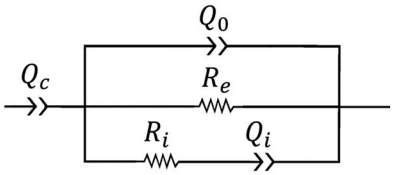

Fig. 10 EEC model used to fit the EIS data.

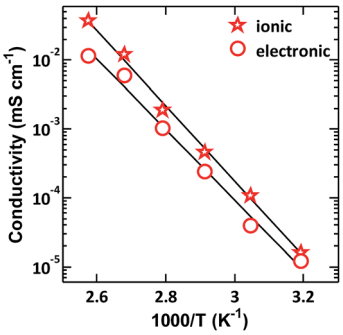

Fig. 11 Arrhenius dependence of the ionic and electronic conductivities of the fully converted film F2 on temperature in the range of 40 to 115 °C; symbols are experimental data, and straight lines are fits to the Arrhenius equation ($R^2 = 0.991$ for the electronic and 0.997 for the ionic conductivity data). The relative uncertainty in the conductivity values, estimated from the relative standard error of the resistance values in the EEC fits and the relative standard error in the thickness measurement, was about 15%.

The electronic and ionic conductivities were calculated using $\sigma = t/(RA)$, where t is the thickness of the film, A is its cross-sectional area, and R is the value of the corresponding resistances, R_e and R_i, determined from the CNLS fits of EIS data.

The electronic and ionic conductivities were calculated to be 1.1×10^{-5} and 2.1×10^{-6} mS cm^{-1}, respectively, at 25 °C. This ionic conductivity is close to that reported by Lin *et al.*[26] for their polyacetylene ionomers consisting of ethyltrimethylammonium triflate and tetramethylammonium ethanesulfonate side groups. However, the electronic conductivities of these ionomers were at least three orders of magnitude lower than the values determined in the present system. The electronic conductivity observed here at 25 °C is similar to that reported by Chiang *et al.*[56] (about 10^{-5} mS cm^{-1}) for undoped, unstretched polyacetylene, synthesized using the Shirakawa method.

Both the electronic and ionic conductivities measured in this work showed an Arrhenius type dependence on temperature (Fig. 11), and increased significantly with an increase in temperature. At 115 °C, the upper bound of the temperature range investigated, the electronic and ionic conductivities were 1.13×10^{-2} and 3.75×10^{-2} mS cm^{-1}, respectively—about 9000 and 18 000 times higher than the corresponding room temperature values.

From the Arrhenius fits, activation energies for electronic and ionic conductivities were determined to be 97.8 ± 13.0 kJ mol^{-1} 104.6 ± 8.2 kJ mol^{-1} respectively. Lin *et al.*[26] found the ionic conduction activation energies of cationically and anionically functionalized polyacetylene ionomers to be 0.94 and 0.97 eV, respectively. In the units of eV, the activation energy for ionic

conduction, for our polyene–IL blends was about 1.08 eV, in good agreement with the values reported by Lin *et al.* for their ionomers.

Conclusions

Hydroiodic acid was found to catalyze the dehydration of PVA at temperatures below 200 °C. The acid-catalyzed dehydration of PVA resulted in the formation of conjugated C=C segments, which in the presence of an imidazolium iodide IL in the film, resulted in simultaneous electronic and ionic conduction. IR, NMR, and Raman spectroscopy, along with EIS analysis, demonstrated the successful preparation as well as the dual-conductivity characteristics of the films. An important drawback in the synthesis of conjugated polymer films using the thermal elimination route is the formation of morphological defects due to internal stresses generated upon volume reduction during conversion. The incorporation of IL in the precursor film greatly alleviated this problem.

The polyene films reported herein, with dual conductivity, are expected to be useful as novel materials for many electrochemical applications. Further doping of the films with iodine, would not only increase the electronic conductivity of the polyene network, but also impart redox activity to the films due to *in situ* formation of iodide/triiodide redox couple. Thermally stable ILs with other anions and cations could similarly be incorporated in the polyene films to obtain functional materials with a wide range of applications.

While this report does not focus on the microstructure of the polyene–IL blend, it is quite likely that the polar IL molecules will form ionic clusters in the relatively nonpolar conjugated polymer matrix. The size and morphology of the aggregates would depend on the concentration of IL in the blend and temperature. A systematic investigation of the film microstructure, and correlating it to the electrical and mechanical properties of the film using the techniques reported herein, seems reasonably warranted.

Acknowledgements

Financial support from Energy Materials Corporation is greatly appreciated. The use of research facilities at the Center for Advanced Materials Processing at Clarkson University, which is supported by the New York State Office of Science, Technology, and Academic Research, is gratefully acknowledged.

References

1 A. Pron and P. Rannou, *Prog. Polym. Sci.*, 2002, **27**, 135–190.
2 C. L. Chochos and S. A. Choulis, *Prog. Polym. Sci.*, 2011, **36**, 1326–1414.
3 W. R. Salaneck, R. H. Friend and J. L. Brédas, *Phys. Rep.*, 1999, **319**, 231–251.
4 K. M. Coakley and M. D. McGehee, *Chem. Mater.*, 2004, **16**, 4533–4542.
5 U. Mitschke and P. Bäuerle, *J. Mater. Chem.*, 2000, **10**, 1471–1507.
6 Y. Sun, Y. Liu and D. Zhu, *J. Mater. Chem.*, 2005, **15**, 53–65.
7 C. Chiang, C. Fincher Jr, Y. Park, A. Heeger, H. Shirakawa, E. Louis, S. Gau and A. G. MacDiarmid, *Phys. Rev. Lett.*, 1977, **39**, 1098–1101.
8 M. Aldissi, *Synth. Met.*, 1984, **9**, 131–141.
9 Y. V. Korshak, V. V. Korshak, G. Kanischka and H. Höcker, *Makromol. Chem., Rapid Commun.*, 1985, **6**, 685–692.
10 C. Marvel, J. Sample and M. F. Roy, *J. Am. Chem. Soc.*, 1939, **61**, 3241–3244.
11 K. Maruyama, M. Také, N. Fujii and Y. Tanizaki, *Bull. Chem. Soc. Jpn.*, 1986, **59**, 13–17.
12 M. Kozlov and T. McCarthy, *Polym. Prepr.*, 2004, **227**, U434–U435.
13 J. H. Edwards and W. J. Feast, *Polymer*, 1980, **21**, 595–596.
14 J. F. Mike and J. L. Lutkenhaus, *J. Polym. Sci., Part B: Polym. Phys.*, 2013, **51**, 468–480.
15 M. E. Abdelhamid, A. P. O'Mullane and G. A. Snook, *RSC Adv.*, 2015, **5**, 11611–11626.
16 L. Wang, X. He, W. Sun, J. Li, J. Gao, G. Tian, J. Wang and S. Fan, *RSC Adv.*, 2013, **3**, 3227–3231.
17 D. Aradilla, G. Bidan, P. Gentile, P. Weathers, F. Thissandier, V. Ruiz, P. Gómez-Romero, T. J. S. Schubert, H. Sahin and S. Sadki, *RSC Adv.*, 2014, **4**, 26462–26467.
18 K. Park, S. B. Schougaard and J. B. Goodenough, *Adv. Mater.*, 2007, **19**, 848–851.
19 H. Zheng, R. Yang, G. Liu, X. Song and V. S. Battaglia, *J. Phys. Chem. C*, 2012, **116**, 4875–4882.
20 A. E. Javier, S. N. Patel, D. T. Hallinan, V. Srinivasan and N. P. Balsara, *Angew. Chem., Int. Ed.*, 2011, **50**, 9848–9851.
21 Z. Siroma, J. Hagiwara, K. Yasuda, M. Inaba and A. Tasaka, *J. Electroanal. Chem.*, 2010, **648**, 92–97.
22 D. Witker and M. D. Curtis, *J. Power Sources*, 2006, **156**, 525–532.
23 N. Costantini, G. Wegner, M. Mierzwa and T. Pakula, *Macromol. Chem. Phys.*, 2005, **206**, 1345–1354.
24 J. Płocharski and H. Wyciślik, *Solid State Ionics*, 2000, **127**, 337–344.
25 X. Ren and P. G. Pickup, *J. Chem. Soc., Faraday Trans.*, 1993, **89**, 321–326.
26 F. Lin, Y. Wang and M. Lonergan, *J. Appl. Phys.*, 2008, **104**, 103517.
27 B. Ringstrand, S. Seifert and M. A. Firestone, *J. Polym. Sci., Part B: Polym. Phys.*, 2013, **51**, 1215–1227.
28 S. Lee, G. A. Becht, B. Lee, C. T. Burns and M. A. Firestone, *Adv. Funct. Mater.*, 2010, **20**, 2063–2070.
29 S. M. Brombosz, S. Seifert and M. A. Firestone, *Polymer*, 2014, **55**, 3370–3377.
30 L. V. N. R. Ganapatibhotla, J. Zheng, D. Roy and S. Krishnan, *Chem. Mater.*, 2010, **22**, 6347–6360.
31 A. Sreeram, N. G. Patel, R. I. Venkatanarayanan, S. J. DeLuca, P. A. Yuya and S. Krishnan, *Polym. Test.*, 2014, **37**, 170–178.
32 J. E. Garland, C. M. Pettit and D. Roy, *Electrochim. Acta*, 2004, **49**, 2623–2635.
33 H. Shirakawa, E. J. Louis, A. G. MacDiarmid, C. K. Chiang and A. J. Heeger, *J. Chem. Soc., Chem. Commun.*, 1977, **16**, 578–580.
34 L. V. N. R. Ganapatibhotla, L. Wu, J. P. Zheng, X. Jia, D. Roy, J. B. McLaughlin and S. Krishnan, *J. Mater. Chem.*, 2011, **21**, 19275–19285.

35 G. A. Arbuckle, N. M. Buecheler and K. G. Valentine, *Chem. Mater.*, 1994, **6**, 569–572.
36 Z. Chen, M. Liu, M. Shi, Z. Shen and D. O. Hummel, *Makromol. Chem.*, 1987, **188**, 2687–2695.
37 S. Saito and M. Tasumi, *J. Raman Spectrosc.*, 1983, **14**, 310–321.
38 M. Mizuno, J. Tanaka and I. Harada, *J. Phys. Chem.*, 1981, **85**, 1789–1794.
39 H. W. Gibson, S. Kaplan, R. A. Mosher, W. Prest and R. J. Weagley, *J. Am. Chem. Soc.*, 1986, **108**, 6843–6851.
40 J. W. Gilman, D. L. VanderHart and T. Kashiwagi, *ACS Symp. Ser.*, 1994, **599**, 161–185.
41 X. Zhang, I. Burgar, E. Lourbakos and H. Beh, *Polymer*, 2004, **45**, 3305–3312.
42 V. Hanková, E. Slováková, J. Zedník, J. Vohlídal, R. Sivkova, H. Balcar, A. Zukal, J. Brus and J. Sedláček, *Macromol. Rapid Commun.*, 2012, **33**, 158–163.
43 T. Moumene, E. H. Belarbi, B. Haddad, D. Villemin, O. Abbas, B. Khelifa and S. Bresson, *J. Mol. Struct.*, 2015, **1083**, 179–186.
44 F. Rodrigues, G. M. do Nascimento and P. S. Santos, *Macromol. Rapid Commun.*, 2007, **28**, 666–669.
45 H. Shirakawa, T. Ito and S. Ikeda, *Polym. J.*, 1973, **4**, 460–462.
46 I. Harada, Y. Furukawa, M. Tasumi, H. Shirakawa and S. Ikeda, *J. Chem. Phys.*, 1980, **73**, 4746–4757.
47 I. Harada, M. Tasumi, H. Shirakawa and S. Ikeda, *Chem. Lett.*, 1978, **7**, 1411–1414.
48 M. Druy, C. Tsang, N. Brown, A. Heeger and A. Macdiarmid, *J. Polym. Sci., Part B: Polym. Phys.*, 1980, **18**, 429–441.
49 M. E. Galvin and G. E. Wnek, *J. Polym. Sci., Part B: Polym. Phys.*, 1983, **21**, 2727–2737.
50 M. F. Rubner, S. K. Tripathy, J. Georger Jr and P. Cholewa, *Macromolecules*, 1983, **16**, 870–875.
51 J. M. Pochan, D. F. Pochan, H. Rommelmann and H. W. Gibson, *Macromolecules*, 1981, **14**, 110–114.
52 R. Huq and G. C. Farrington, *J. Electrochem. Soc.*, 1984, **131**, 819–823.
53 R. A. Huggins, *Ionics*, 2002, **8**, 300–313.
54 J. Jamnik and J. Maier, *J. Electrochem. Soc.*, 1999, **146**, 4183–4188.
55 Y. H. Jang, J. R. Barber and S. J. Hu, *J. Phys. D: Appl. Phys.*, 1998, **31**, 3197–3205.
56 C. K. Chiang, *Phys. A*, 2003, **321**, 139–151.

Supplementary Information

Simultaneous Electronic and Ionic Conduction in Ionic Liquid Imbibed Polyacetylene-Like Conjugated Polymer Films

Arvind Sreeram,[a] Sitaraman Krishnan,*[a] Stephan J. DeLuca,[b] Azar Abidnejad,‡[a] Michael C. Turk,[c] Dipankar Roy,[c] Elham Honarvarfard[d] and Paul J. G. Goulet[d]

[a] Department of Chemical and Biomolecular Engineering, Clarkson University, Potsdam, New York, 13699, USA. E-mail: skrishna@clarkson.edu; Fax: +1-315-268-6654; Tel: +1-315-268-6661
[b] Energy Materials Corporation, Norcross, Georgia, 30071, USA
[c] Department of Physics, Clarkson University, Potsdam, New York, 13699, USA
[d] Department of Chemistry and Biomolecular Science, Clarkson University, Potsdam, New York, 13699, USA
‡ Currently at Solvay USA Inc., Vernon, Texas, 76384, USA

Film surface morphology. Scanning electron microscopy of the ionic liquid containing conjugated polymer film showed a relatively uniform surface (see Fig. S1). No droplets of IL were evident on the film surface.

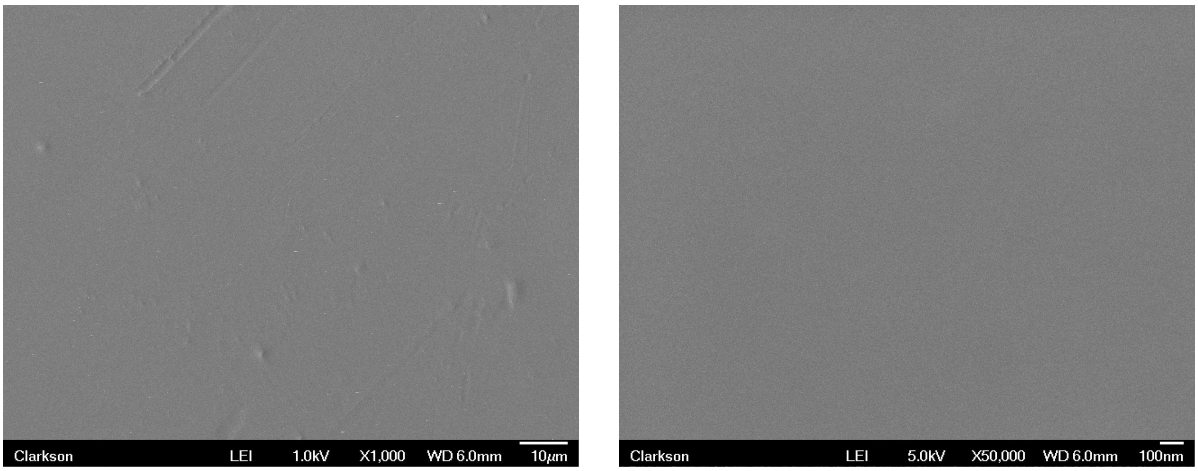

Fig. S1 Low magnification (1000×, left) and high magnification (50,000×, right) SEM images of film F2 after reaction at 200 °C. A photograph of the film is shown in Fig. 5 of the main article.

Detailed analysis of electrochemical impedance spectroscopy data. The electrical equivalent circuit (EEC) determined from the experimental impedance data is shown in Fig. 10 of the main article and is reproduced here.

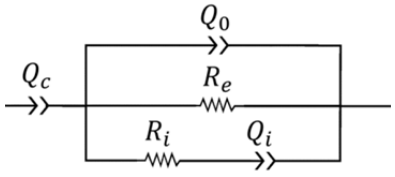

The values of the parameters associated with the main elements of this circuit (Q_0, R_e, R_i and Q_i) are summarized in Table S1. Y_0 and n_0 are parameters of the geometric constant phase element (CPE), Q_0, and serve to define the impedance, $Z(Q_0)$, of the CPE as $Z(Q_0) = 1/[Y_0(j\omega)^{n_0}]$, where $j = \sqrt{-1}$. Likewise, Y_i and n_i are the CPE parameters of Q_i, and this CPE has the impedance, $Z(Q_i) = 1/[Y_i(j\omega)^{n_i}]$. Both the resistances, R_e and R_i, increase with decreasing temperatures, and the CPE parameters also show their expected temperature dependent behaviors.[1]

Table S1 Temperature variation of the parameters of the EEC model determined by complex nonlinear least squares (CNLS) fitting of the EIS data acquired at 7 different temperatures.

T (°C)	115	100	85	70	55	40	25
$Y_0 \times 10^4$ ($\mathrm{mS\ s}^{n_0}$)	5.62	17.6	25.8	5.73	1.09	0.293	0.156
n_0	0.5467	0.4935	0.4221	0.4794	0.5552	0.6059	0.5893
R_e (kΩ)	1.052	1.998	11.58	50.27	301.7	991.7	8224.0
R_i (kΩ)	0.319	0.979	6.33	26.06	109.9	741.3	5822.9[(a)]
$Y_i \times 10^4$ ($\mathrm{mS\ s}^{n_i}$)	2480	4800	107	72.2	38.5	5.78	n.d.[(a)]
n_i	0.4065	0.6705	0.6022	0.4575	0.3074	0.3093	n.d.[(a)]
f_{0e}(kHz) [(b)]	127.9	14.96	0.6537	0.2599	0.07517	0.05468	0.005209

[(a)] not determined. At 25 °C, the net impedance of the R_i-Q_i branch was much larger than the net impedance of the Q_0-R_e parallel combination, and hence could not be adequately resolved by CNLS fitting of the experimental data. However, the Q_0-R_e unit was fully resolved at this temperature, and the corresponding parameter values are shown in the table. The value of R_i at 25 °C was determined by the method of extrapolation.

[(b)] Characteristic frequency of the Q_0-R_e subunit of the EEC. See the discussion that follows.

The impedance parameters shown in the last column of Table S1 are comparable, in their respective orders of magnitudes, to those previously reported for similar experimental systems involving mixed electronic and ionic conducting materials.[2,3] The power-factor (n_0 or n_i in the present case) of the CPE varies between 0 and 1, with purely resistive and purely capacitive behaviors of the element emerging at these bounds, respectively.[4] At a value of 0.5, this parameter represents a Warburg diffusion element.[5] Based on the n_i values listed in Table S1, we identify the CPE, Q_i, to be a Warburg-like diffusion element, which along with the circuit element R_i, represents diffusion of ions. Because the current collector electrodes are ionically blocking, the ion transport should correspond to the case of restricted diffusion with reflective boundaries.[6] Nevertheless, the observed CPE signature of Warburg-like semi-infinite diffusion implies that the diffusion frequency of the charge carriers is small compared with all the perturbation frequencies used for EIS.[7] The observed deviations of n_i from the value of 0.5 (expected for

an ideal Warburg element) is attributed to inhomogeneous distribution of diffusion sites in the sample.[6,8]

Unlike the case of ions, electron transport in our measurements is associated with non-blocking boundaries, and therefore, the parameters of the ("electron leaking") geometric CPE, Q_0, are affected by the diffusive movements of electrons. The expected Warburg-like nature of Q_0 is validated by the values of n_0, observed in the neighborhood of 0.5, as expected for a Warburg element. It is likely that, this Q_0 is a parallel combination of the actual geometric CPE with a Warburg-like CPE resulting from electron diffusion. The latter is expected to dominate the resulting value of such a combination, because the intrinsic Y_0 for these systems tends to be rather small (typically in the range between 10^{-11} and 10^{-9} S s^n),[2,3] which makes the innate impedance of the geometric CPE very large. The effect of electron diffusion on the value of Y_0 is also suggested by the observed increase in the value of this parameter with temperature, consistent with an expected increase in the diffusion coefficient with an increase in temperature.

As seen in Fig. 9 of the main article, the Nyquist spectra recorded at the moderate temperatures displayed two visually separable impedance arcs formed by the $Q_0(R_e)$ and the (Q_iR_i) subunits of the EEC. The specific circuit-blocks linked to these individual arcs can be identified from a careful examination of the characteristic frequencies (or time constants) of the arcs. For a simple parallel combination of a resistor and a CPE, the characteristic frequency would appear at the top (maximum $-Z''$) of the depressed semicircle generated by the combined elements.[9] However, with the mutually overlapping arcs observed in the present work, it was difficult to clearly locate these characteristic frequencies by simple inspection.

Therefore, in order to identify the electronic and ionic components of the recorded Nyquist plot at each temperature setting, we evaluated the characteristic frequency of the $Q_0(R_e)$ block using the CNLS-fitted parameters. Subsequently, we traced the observed frequency spectrum to locate the position of the corresponding data point (labeled by its frequency coordinate) on the given plot. The $Q_0(R_e)$ subunit of the EEC was specifically chosen for this analysis, because the impedance parameters of this block were fully resolved in the CNLS fits at all temperatures of measurement (Table S1). In addition, this combination of elements would lead to a well-defined, and hence readily identifiable, semicircle with whose center is located at an angle of $[(1-n_0)\pi/2]$ below the Z' axis. Once the Nyquist feature for this impedance contribution of electronic conduction was identified, the remaining Nyquist feature could be readily linked to ionic conduction.

The time constant (τ_{0e}) and the corresponding characteristic frequency (f_{0e}) of the $Q_0(R_e)$ combination were calculated using:[9]

$$\tau_{0e} = (Y_0R_e)^{1/n_0} = (2\pi f_{0e})^{-1}$$

Fig. S2 shows the temperature dependent variation of f_{0e}, calculated using the above equation and the CNLS-fitted values of Y_0 and R_e from Table S1. The observed increase in f_{0e} with an increase in temperature is dominated by the thermal response of R_e (which decreases with temperature), and this is consistent with previously reported behaviors for such relaxation frequencies.[10] For all the Nyquist spectra, acquired at the seven different temperatures, the impedance data points corresponding to the calculated values of f_{0e} were found to be located on the arcs at the high-frequency end (left side) of the spectrum.

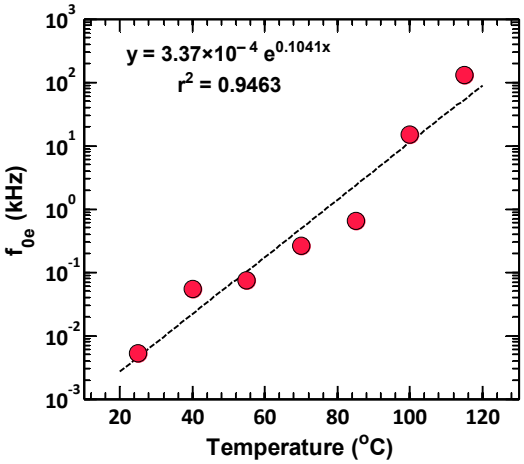

Fig. S2 Temperature dependence of the characteristic frequency, f_{0e}, of the Q_0-R_e impedance unit in the EEC. The symbols represent data points obtained by CNLS fitting the experimental impedance data, and the solid trace is the best-fit curve for the f_{0e} vs. temperature data. The equation used and the overall quality of the fit (r^2 value) are indicated in the figure.

On the basis of this analysis, it was concluded that the arc associated with the higher frequency data (left side of the Nyquist spectrum) in Fig. 9 was linked to electronic conduction, while the arc corresponding to the lower frequency data (on the right side of the Nyquist plot) was associated with ionic conduction.

Shape of the Nyquist spectra acquired at 115 °C. The radius of the arc attributed to the electronic conduction is proportional to R_e.[9] From the values of R_e given in Table S1, it is evident that the radius of this arc would decrease with an increase in temperature. Simultaneously, because of an increase in f_{0e} with temperature (cf. Fig. S2), the top of the arc would shift toward the left of the Nyquist spectrum, carrying with it the entire arc. At 115 °C, the top of the electronic arc was located at impedance values corresponding to 128 kHz, and therefore, at the very left end of the $+Z'$ axis. (Note that the last experimental data point observed at the left-most end of the $+Z'$ axis in each panel of Fig. 9 was from a measurement using a perturbation frequency of 300 kHz). As a result, only a small portion of the $Q_0(R_e)$ arc was revealed in our measurements (see the high-frequency corner of the Nyquist spectrum in Fig. 9D), while the remaining plot area was covered by the arc resulting from ionic conduction. Note also that the overall dimension of the ionic arc was significantly smaller for the spectrum acquired at 115 °C, compared with the ionic arcs observed in the lower temperature spectra. However, on the optimized impedance scale used in Fig. 9D, the Nyquist feature of the ionic rail appears to dominate the observed spectrum. In conclusion, the impedance spectrum collected at 115 °C was predominantly the signature of the of the ionic rail, whereas the spectrum acquired at 25 °C was, for most part, a manifestation of the electronic rail. The spectra acquired at intermediate temperatures displayed impedance features from both, the electronic and the ionic transport pathways.

References

1. J. R. Macdonald, Solid State Ionics, 1984, **13**, 147–149.
2. M. Wasiucionek, J. Garbarczyk, B. Wnętrzewski, P. Machowski and W. Jakubowski, Solid State Ionics, 1996, **92**, 155–160.
3. E. S. Matveeva, R. D. Calleja and V. Parkhutik, J. Non-Cryst. Solids, 1998, **235**, 772–780.
4. J. Jorcin, M. E. Orazem, N. Pébère and B. Tribollet, Electrochim. Acta, 2006, **51**, 1473–1479.
5. E. Cuervo-Reyes, C. P. Scheller, M. Held and U. Sennhauser, J. Electrochem. Soc., 2015, **162**, A1585–A1591.
6. J. Bisquert, J. Phys. Chem. B, 2002, **106**, 325–333.
7. J. Garland, D. Crain and D. Roy, Electrochim. Acta, 2014, **148**, 62–72.

8. J. Bisquert and A. Compte, J. Electroanal. Chem., 2001**, 499**, 112–120.
9. G. J. Brug, A. L. G. Van Den Eeden, M. Sluyters-Rehbach and J. H. Sluyters, J. Electroanal. Chem., 1984, **176**, 275–295.
10. J. R. MacDonald, Solid State Ionics, 1985, **15**, 159–161.